SAND REPORT
SAND2002-0082
Unlimited Release
Printed January 2002

Experimental Comparison of 2-3MV X-ray Sources for Flash Radiography

Peter R. Menge, David L. Johnson, John E. Maenchen, Craig L. Olson, and Dean C. Rovang

Prepared by
Sandia National Laboratories
Albuquerque, New Mexico 87185 and Livermore, California 94550

Sandia is a multiprogram laboratory operated by Sandia Corporation, a Lockheed Martin Company, for the United States Department of Energy under Contract DE-AC04-94AL85000.

Sandia National Laboratories

Issued by Sandia National Laboratories, operated for the United States Department of Energy by Sandia Corporation.

Available to DOE and DOE contractors from
U.S. Department of Energy
Office of Scientific and Technical Information
P.O. Box 62
Oak Ridge, TN 37831

Telephone: (865)576-8401
Facsimile: (865)576-5728
E-Mail: reports@adonis.osti.gov
Online ordering: http://www.doe.gov/bridge

Available to the public from
U.S. Department of Commerce
National Technical Information Service
5285 Port Royal Rd
Springfield, VA 22161

Telephone: (800)553-6847
Facsimile: (703)605-6900
E-Mail: orders@ntis.fedworld.gov
Online order: http://www.ntis.gov/ordering.htm

SAND2002-0082
Unlimited Release
Printed January 2002

Experimental Comparison of 2-3MV X-ray Sources for Flash Radiography

Peter R. Menge, David L. Johnson, John E. Maenchen,
Craig L. Olson, and Dean C. Rovang
Radiographic Physics
Sandia National Laboratories*
P.O. Box 5800
Albuquerque, NM 87185-1193

Darryl Droemer and Eugene Hunt
Bechtel-Nevada
Las Vegas, NV

Bryan Oliver, Dave Rose, and Dale Welch
Mission Research Corporation
Albuquerque, NM 87110

Abstract

High-brightness flash x-ray sources are needed for penetrating dynamic radiography for a variety of applications. Various bremsstrahlung source experiments have been conducted on the TriMeV accelerator (3MV, 60 Ω, 20 ns) to determine the best diode and focussing configuration in the 2-3 MV range. Three classes of candidate diodes were examined: gas cell focussing, magnetically immersed, and rod pinch. The best result for the gas cell diode was 6 rad at 1 meter from the source with a 5 mm diameter x-ray spot. Using a 0.5 mm diameter cathode immersed in a 17 T solenoidal magnetic field, the best shot produced 4.1 rad with a 2.9 mm spot. The rod pinch diode demonstrated very reproducible radiographic spots between 0.75 and 0.8 mm in diameter, producing 1.2 rad. This represents a factor of eight improvement in the TriMeV flash radiographic capability above the original gas cell diode to a figure of merit (dose/spot diameter^2) > 1.8 rad/mm^2. These results clearly show the rod pinch diode to be the choice x-ray source for flash radiography at 2-3 MV endpoint.

Acknowledgements

The authors are grateful for the engineering, technical expertise and operational assistance provided by J. Gustwiller, I. Molina, D. Nelson, and R. Shear of Sandia, E. Ormand and L. Woo of Bechtel-Nevada, and S. Cordova of Ktech Corp. Valuable discussions were conducted with G. Cooperstein, R.J. Commisso, and S.B. Swanekamp of the Naval Research Laboratory. The programmatic support provided by G. MacLeod of Bechtel-Nevada is greatly appreciated.

Contents

Experimental Comparison of 2-3MV X-ray Sources for Flash Radiography

I. Introduction

X-ray sources for dynamic radiography need to be fast pulsed (<100 ns) to freeze motion blur, small in spatial extent to maximize resolution, and intense to overcome noise and achieve adequate Poisson statistics in the imaging detector. Furthermore, they should be appropriately spectrum matched to the object thickness and material to optimize contrast. Various pulsed electron accelerators have been built worldwide by national laboratories and industry to create bremsstrahlung sources to accomplish these radiographic tasks[1-8]. Various focussing schemes have been employed to provide the smallest bremsstrahlung spot possible while still preserving enough dose to accomplish the radiographic task. These focussing techniques include multipole magnet[1,2,4], immersed solenoid magnet[6,9], gas cell[3,10-12], self pinch[13,14], anode cone[7,8], and rod pinch[15,16]. When developing a radiographic source with a 3 MeV endpoint, the best choice of focussing technique for this energy was not known a priori. Candidate techniques were chosen for evaluation on a common accelerator, TriMeV[12]. TriMeV is a pulsed power accelerator designed to produce a 3 MV negative (2MV positive), 20 ns pulse ($\approx$ 4 ns rise time) with a 60 Ω drive impedance. It uses a Marx generator to charge an oil-filled three stage pulse forming line (PFL). The pulse from the PFL is fed through an intermediate increased-impedance oil coax and vacuum insulator onto a 2.4 m long 60 Ω coaxial vacuum transmission line. The center conductor of the transmission line is anodized aluminum, which does not emit electrons when pulsed negatively up to 3.3 MV. A schematic of the TriMeV accelerator is shown in Figure 1.

Three candidate focussing techniques were chosen for evaluation on TriMeV. Gas cell, immersed solenoid, and rod pinch. These were chosen because all were adaptable to TriMeV and computer simulations[17] and other analyses indicated these to be the most promising for this accelerator. To achieve sufficient dose at 3 MV, high current (10s of kA) is required. Multipole magnet focussing is only useful for low emittance beams with good energy uniformity[18]. Typical

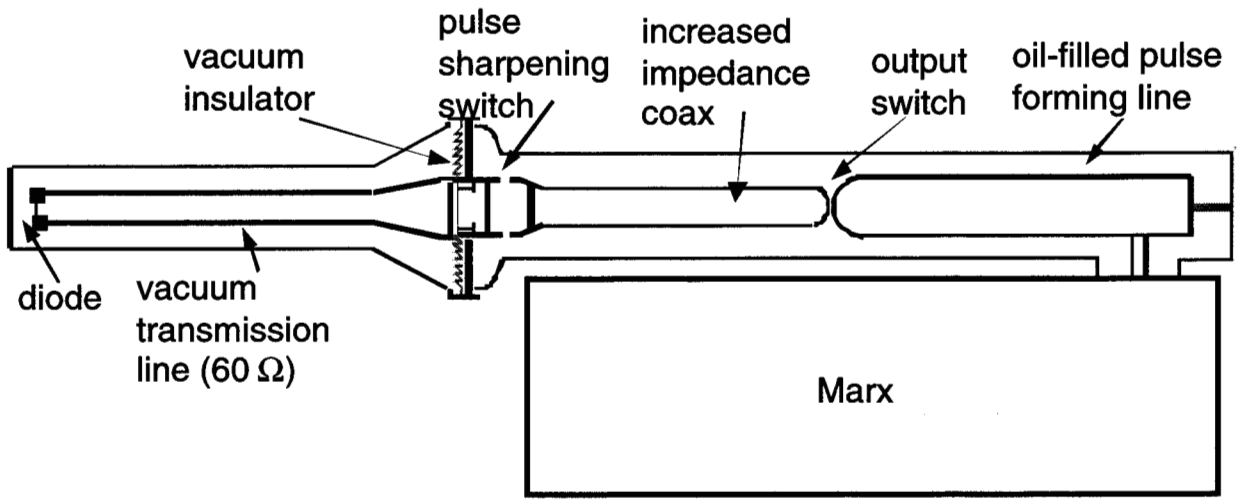

Figure 1. Schematic of the TriMeV accelerator (total length = 7.4 m).

pulsed power high current electron beam generation methods do not provide the requisite emittance or energy uniformity to use this technique. The chosen performance criterion for comparison is a Figure of Merit (FOM) similar to that proposed by Martin[19]. It is:

$$FOM = \frac{D}{s^2} \qquad (1)$$

where D is the x-ray dose in rads at 1 m from the source and filtered by 2.5 cm of aluminum, and s is the effective x-ray spot diameter in mm. The effective diameter is defined as the diameter of a uniform circular area whose modulation transfer function (MTF) shares the same half-maximum as the x-ray spot in spatial frequency coordinates[20]. In other words, the x-ray spot size is the size of a circular area source that can provide the same spatial resolution at 50% modulation. This definition will calculate larger spot sizes than most other conventions. For example, if the spot profile has a Gaussian distribution with a 1 mm effective diameter, then it will have a 0.63 mm FWHM, or a 0.75 mm root mean square (rms) diameter. This criterion reflects the traditional radiography goals of smaller spot and more dose and equitably compares spatial resolution and image intensity of a hypothetical radiograph from any of the three sources, since using a common driver ensures that photon energy endpoint and spectrum will be nearly the same.

II. Gas Cell Focussing Diode

A. Focussing Mechanisms

In the gas cell focusing diode electrons are propagated through a gas-filled cylinder or cone. When the cell is filled to an appropriate pressure, the beam electrons collisionally ionize the gas. Provided enough beam current density, the plasma electrons are ejected radially out of the beam envelope by the beam space charge until the positive ion space charge nearly cancels that of the beam. If the pressure is low enough (a few Torr) the beam will be almost completely charge neutralized but only fractionally current neutralized. The beam's azimuthal magnetic field will cause the beam to contract and undergo betatron orbits about the axis. Typically, the beam

will have its smallest diameter at the first focus at the first quarter-wave betatron wavelength. This process is termed quarter-wavelength focussing.

If the pressure is raised (10 - 20 Torr) then the gas breakdown will form a higher density, more conductive plasma. A plasma current can then flow opposite to the beam current if the plasma's magnetic decay time is long compared to the pulse length[21]. Under this condition of current neutralization, electrons will follow ballistic trajectories determined by their injection angle into the gas since the E and B forces are balanced. If the injection angles are tailored to a converging geometry, the beam will reach a minimum diameter at an appropriately placed bremsstrahlung target. This process is termed ballistic focusing.

The advantages of gas cell focussing are that no magnets are required and relatively high currents and thus, high dose can be achieved. Its disadvantages are that it is relatively difficult to configure, the beam can acquire a relatively high transverse temperature during focussing that reduces the dose[22], and beam non-uniformities can cause spot enlargement instabilities.

B. Experimental arrangement

Figure 2 shows the diode configuration, and diagnostic locations for gas cell focussing experiments. TriMeV was operated in negative polarity (center conductor negative) for the gas cell focussing experiments. The electrons are emitted from a circular velvet cathode (75 mm diameter) recessed in an Pierce type electric field-shaper[23]. The anode is a 0.125 mm thick Ti foil which also serves as the entrance to the gas cell (55 mm diameter). The x-ray converter is a 0.5 mm thick disk of Ta (15 mm diameter) backed by a 1 cm thick graphite beam stop. The gas cell slides to adjust the AK gap. The x-ray converter slides within the gas cell to adjust the drift length. Also shown in Fig. 2 are the locations of the voltage and current monitors. Two voltage monitors, VD, placed 180° apart at this position are capacitive displacement current monitors (D-dots[24]), and two current monitors, ID, also placed 180° apart are B-dot monitors[24]. A resistive shunt foil monitor[25] surrounds the bremsstrahlung target to measure net current in the gas cell, IGC.

The x-ray dose and dose rate are measured with CaF_2 thermoluminescent dosimeters (TLDs) and calibrated PIN diodes, respectively, placed outside the vacuum wall at several distances and angles from the source. There is 2.5 cm of Al filtering between the source and the on-axis dose diagnostics.

The x-ray spot size was determined through analysis of the spot's edge spread function[9,13]. Two edge spreads were measured per experiment. Both used tungsten rolled edges (r = 50 cm) placed 30 - 50 cm from the bremsstrahlung target with one edge standing vertically on-axis and the

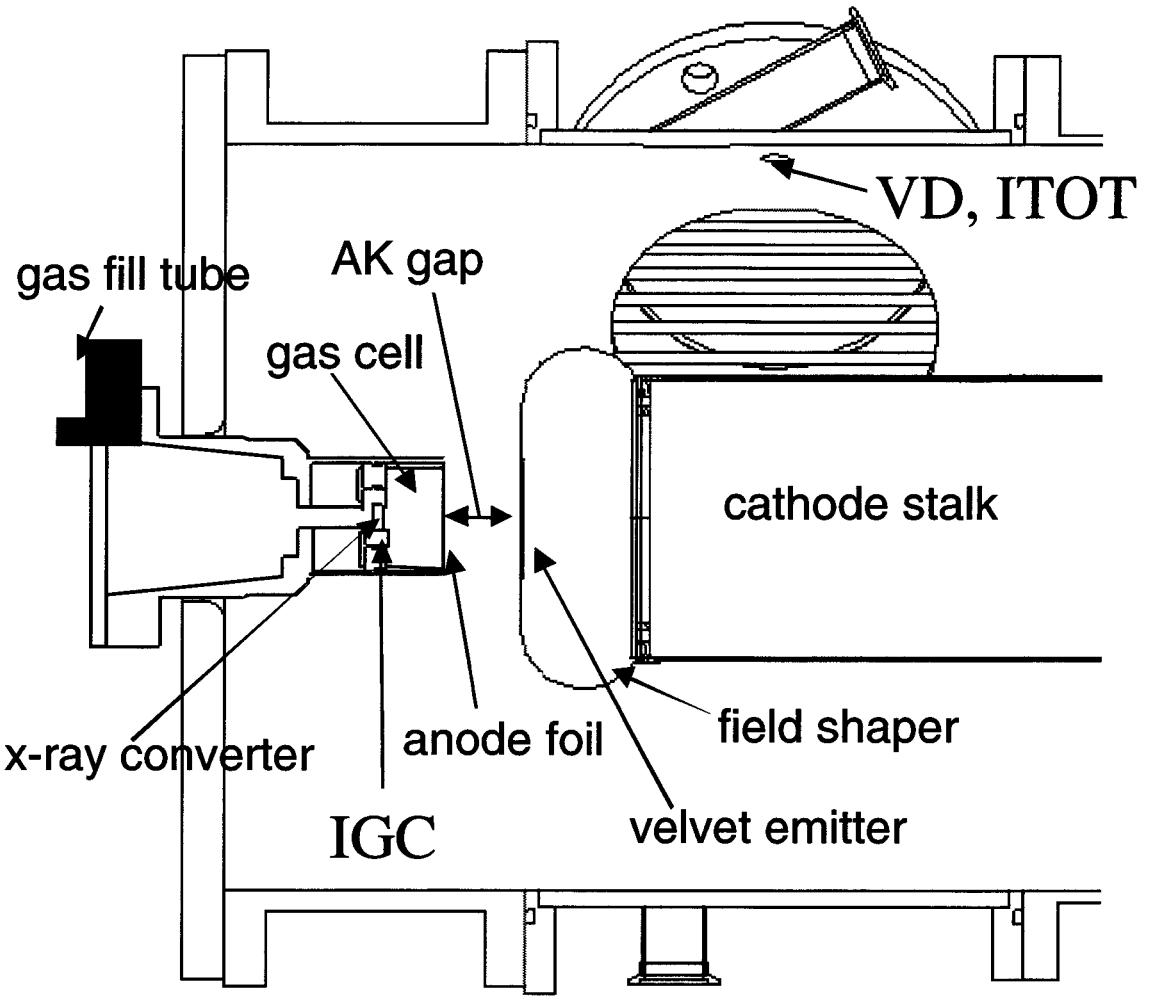

Figure 2. Schematic of TriMeV's gas focussing diode showing the end of the 60 Ω transmission line, the gas cell configuration and the location of the electrical diagnostics (VD, ID, and IGC).

other laid horizontally. The time integrated edge spread images were recorded on x-ray film (Kodak Industrex AA and Fuji 150) interleaved among three 0.5 mm thick lead sheets, placed 150 - 200 cm from the rolled edges, and digitized with a micro-densitometer or calibrated optical scanner.

An example of the edge spread spot size analysis is shown in Figure 3. A Monte Carlo simulation[26] of the bremsstrahlung produced by a circular, 2 mm diameter, 3 MeV electron beam was performed using the geometry shown in Fig. 2. The details of gas focussing were ignored and the cold electron beam simply struck the x-ray converter and the resultant x-rays were followed. A simulated tungsten rolled edge was placed at 50 cm from the bremsstrahlung target, and the resulting bremsstrahlung radiation profile was recorded at 200 cm from the rolled edge, giving a 4× source magnification. The ordinate corresponds to exposure on a piece of hypothetical x-ray film in units of expected dose per coulomb of electron beam charge. The radiation profile on the left side of the graph is in the full radiation field, while the right side is attenuated by the tungsten edge. The transition region contains the spot size information. A simple method to find the effective spot size diameter is found in Ref. 20, and is demonstrated in

Fig. 3. This method well approximates the effective spot diameter as defined in Section I for a wide variety of spot profile distributions such as a uniformly filled circle (this example), Gaussian, Bennett, or annular. The distance between points marking 87.5% and 12.5% of maximum exposure is multiplied by 1.57 and divided by the magnification to yield an effective source diameter of 2.0 mm.

Information on the time resolved spot size was gathered with horizontal and vertical lines of silicon PIN diodes (Quantrad-50) placed behind the film pack. Each line contained 19 individually calibrated PIN diodes with a center-to-center spacing of 3.8 mm. This diagnostic sampled the time resolved edge spread function by comparing the relative intensity of the PIN diode signals at each digitized point in time. Its accuracy is limited to approximately the center-to-center spacing divided by the radiographic magnification.

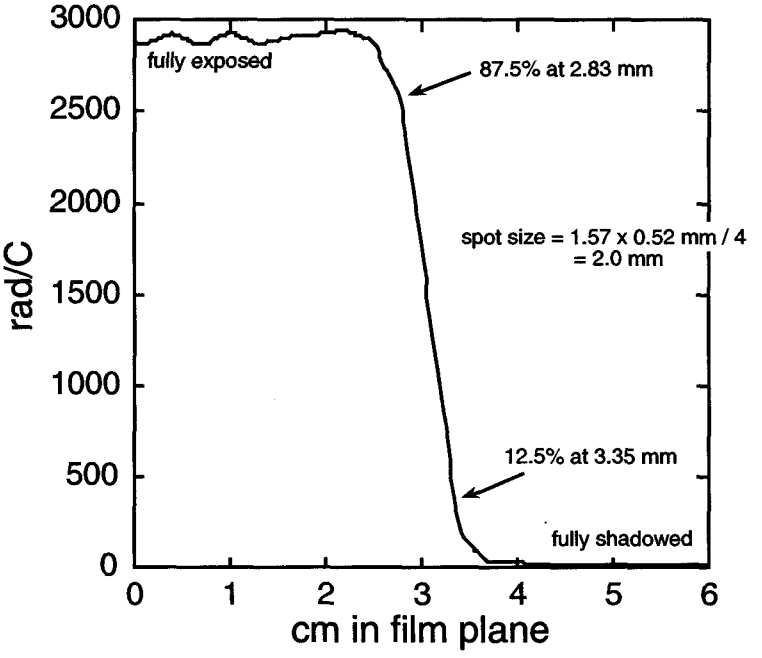

Figure 3. Monte Carlo simulation of a rolled edge x-ray spot size measurement. The bremsstrahlung from a 3 MeV, 2 mm diameter electron beam creates a 2 mm effective diameter x-ray spot.

C. Quarter-Wavelength Focussing Data and Discussion

Sample data recorded with these diagnostics from a typical quarter-wavelength focussing experiment is shown in Figures 4 and 5. This experiment used a 4 cm AK gap, a 2.5 cm gas drift length (distance from target to anode foil), and the cell was filled with 1 Torr of N_2. These parameters were chosen with guidance from computer simulations using IPROP[21], a hybrid kinetic-fluid code which models both vacuum flow and gas breakdown. Figure 4a displays the

diode voltage (VD), injected current (ID), and net current in the gas cell (IGC). Note that the net current is almost indistinguishable from the injected beam current, indicating no current neutralization by the gas. The main pulse ends around 27 ns. The subsequent rising of the voltage and current is the power pulse reflecting back off the vacuum/oil interface at the upstream end of the vacuum transmission line. Fig. 3b shows the x-ray pulse (integrated dose = 3.4 rad at 1 m from the bremsstrahlung target) and the diode impedance (Zdiode = VD/ID).

Figure 5 shows the data from the time-resolved spot size diagnostic. Fig. 5a displays the relative signals from the horizontal line of 19 PIN diodes. Those showing little or no signal are in the shadow of the rolled edge, those of intermediate amplitude are only partially illuminated by the x-ray spot, and those of highest amplitude are fully illuminated. Time slices of this data are analyzed to get a history of the spot size evolution as shown in Fig. 5b. Note that the spot follows the rise and fall of the voltage. The uncertainty in this measurement is approximately ±0.5mm. A dose rate weighted average of these points yields a 4.9 mm spot size in the vertical and 4.5 mm in the horizontal, in rough agreement with the 5.0 mm time-integrated spot measured in both directions by the x-ray film. A 5 mm spot gives FOM = 0.14.

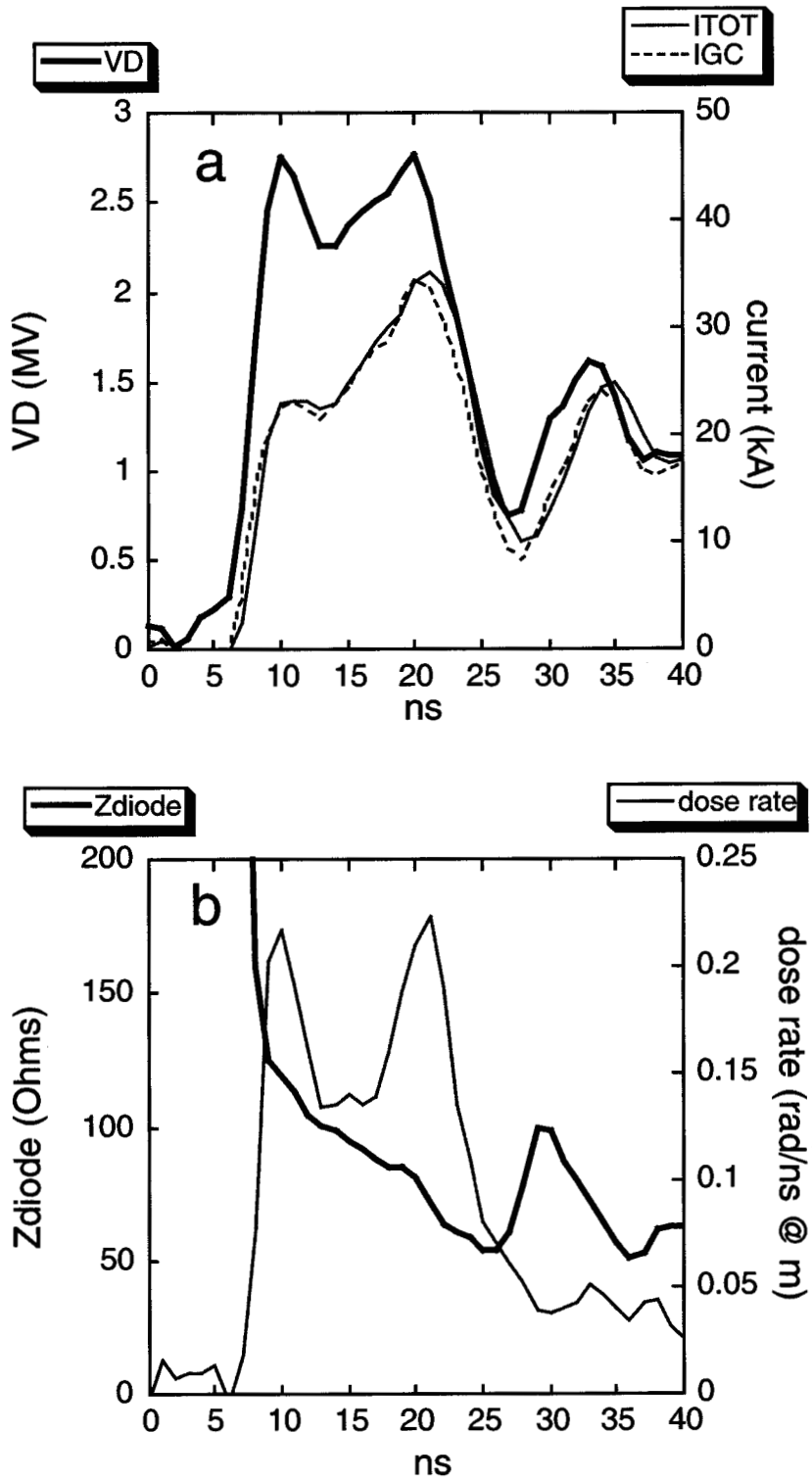

Figure 4. Sample data from a quarter-wavelength focussing shot. a) diode voltage (VD, thick line), diode current (ID, thin solid line), and net current in the gas cell (IGC, thin dashed line). b) diode impedance (Zdiode = VD/ID, thick line), and x-ray pulse 1 m from the source (rad/ns, integrated dose = 3.4 rad).

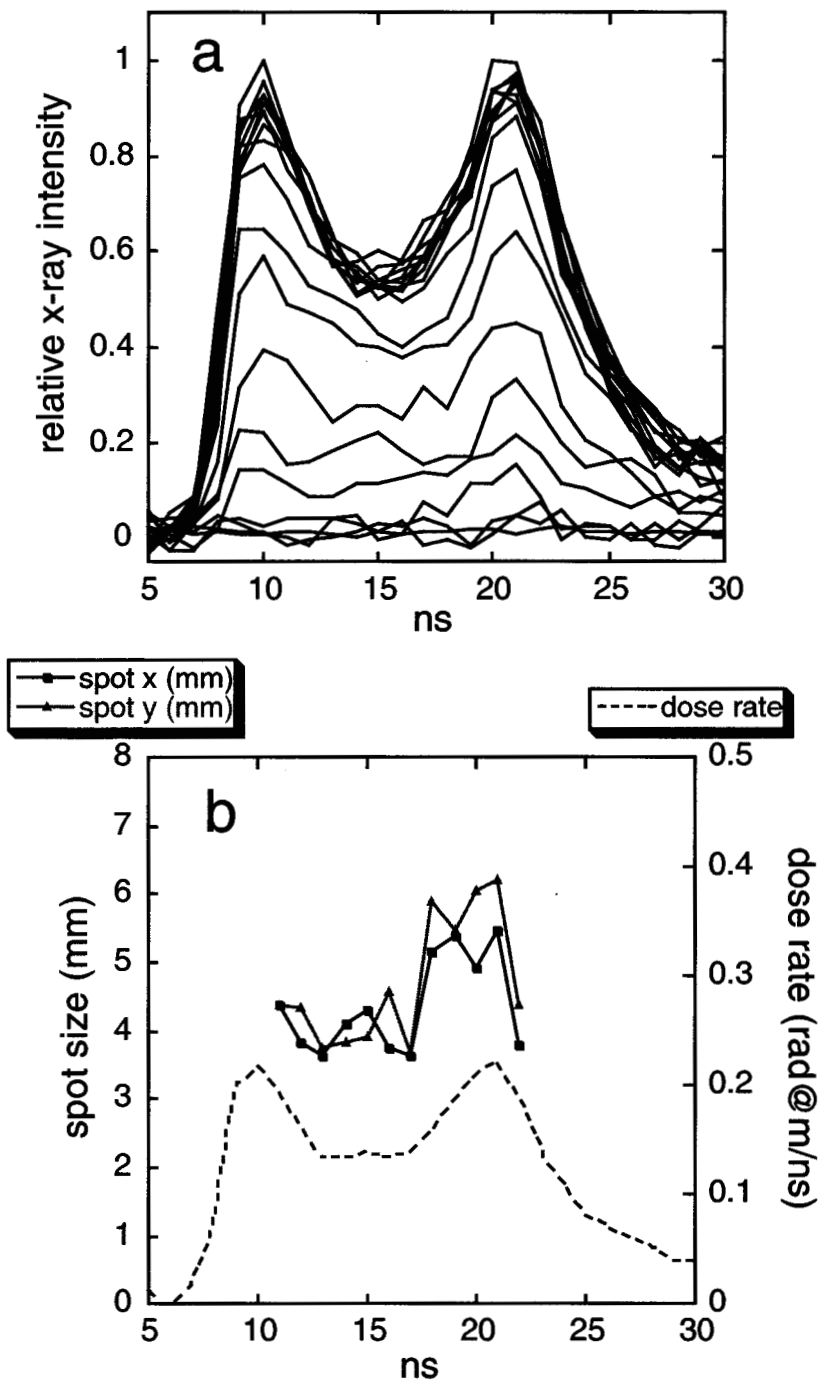

Figure 5. PIN diode data from the time-resolved spot size measurement. a) the 19 PIN diode waveforms which construct a time-resolved edge spread function measuring the vertical diameter of the spot. b) the unfolded time-resolved horizontal (spot x, solid black line) and vertical spot diameters (spot y, solid gray line). Also plotted is the dose rate from Fig. 4b to show relative timing. The time-integrated spot measured from film is 5.0 mm in both directions.

A 2.5 cm drift length was chosen to match the first betatron focus predicted from IPROP simulations. Other lengths were tested to verify that a 2.5 cm drift length produced the minimum spot size. Figure 6 plots the spot sizes for drift lengths of 2.25, 2.5 and 2.75 cm and shows that 2.5 cm must be near the minimum.

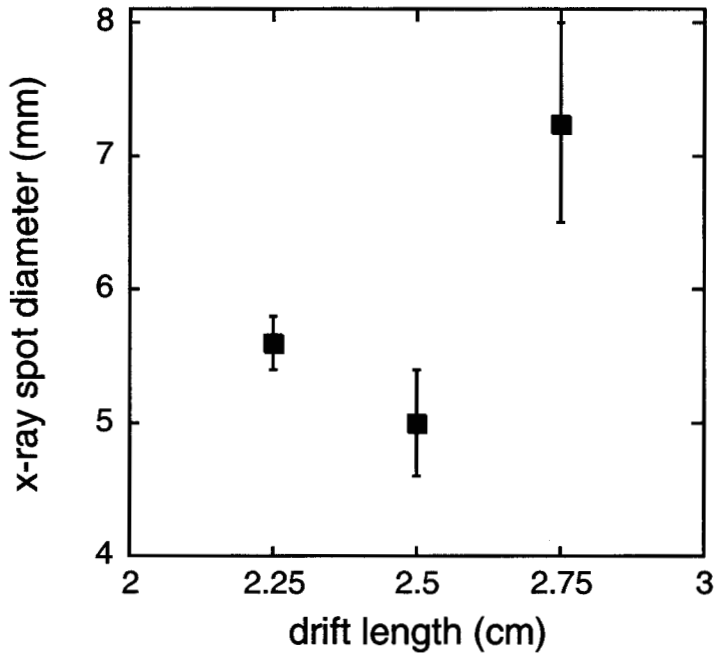

Figure 6. Effect of gas cell drift length on x-ray spot diameter for quarter-wavelength focussing. The spot is minimized near a length of 2.5 cm in agreement with simulation predictions from the IPROP code.

D. Ballistic Focussing Data and Discussion

Sample data from a ballistic focussing experiment is shown in Figure 7. This experiment used a 4 cm AK gap and a 4 cm drift length. The drift length is longer than that used in the quarter-wavelength focussing due to the slower radial convergence created by this mechanism. The gas cell was filled with 10 Torr N_2. Figure 7a displays the diode voltage (VD), injected current (ID), and net current in the gas cell (IGC). Note that in this case the net current is only a few percent of the injected current indicating that the beam current is almost neutralized, and thus, the E and B forces on the beam are minimized. Fig. 7b shows the x-ray pulse (integrated dose = 6.0 rad at 1 m), and the time resolved vertical spot size. The horizontal spot was not measured on this shot but is assumed to be similar to the vertical. The beginning of the x-ray pulse does not follow the voltage like in Fig. 4, because front of the beam is partially eroded away while breaking down the denser gas. The average of the dose rate weighted spot from the time-resolved spot waveform is 5.1 mm, which is the same as the time-integrated spot measured on film. The FOM for this shot is 0.23.

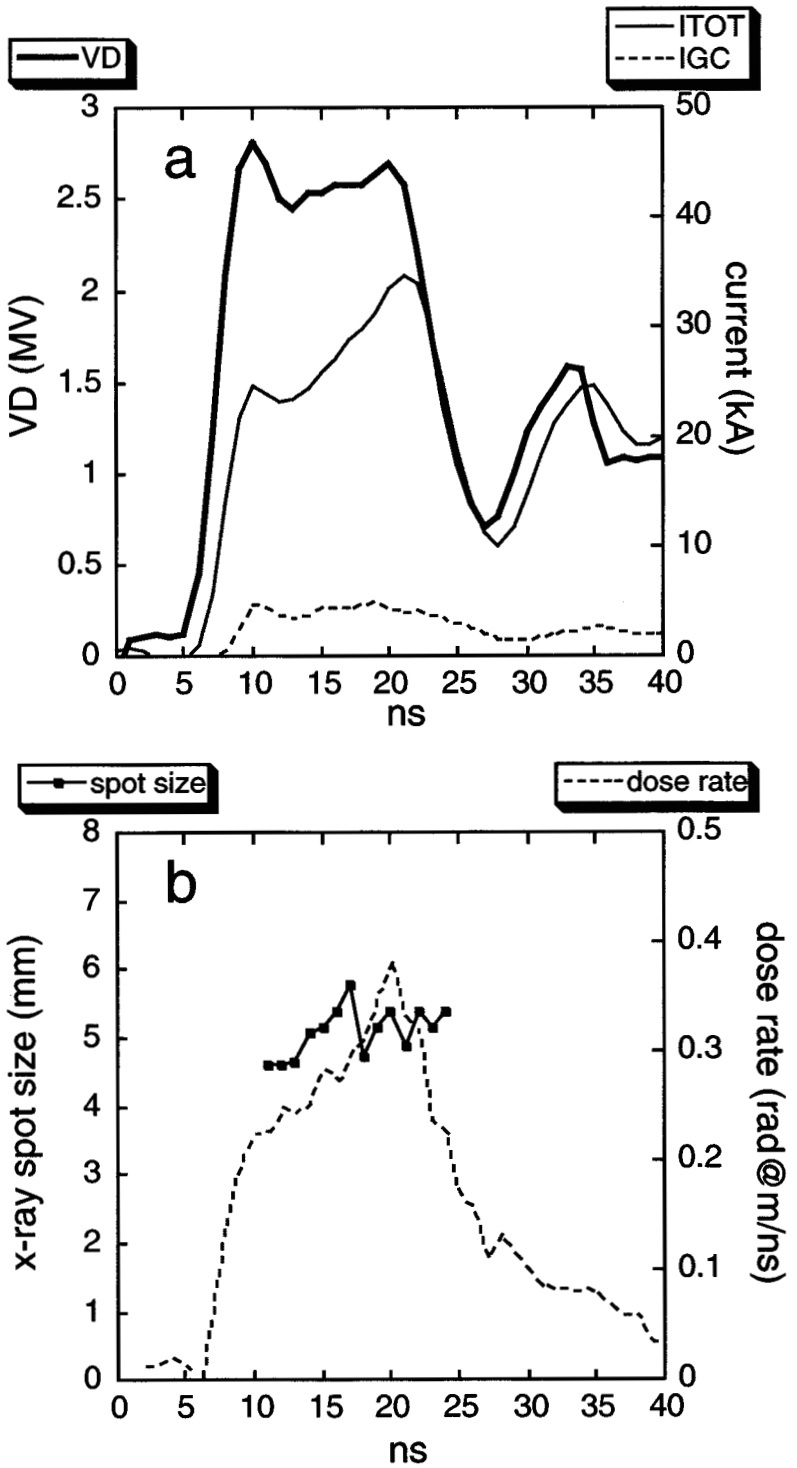

Figure 7. Sample data from a ballistic focussing shot. a) the diode voltage (VD, thick line), diode current (ID, thin solid line), and the net current in the gas cell (IGC, thin dashed line). b)

the x-ray pulse (dose rate, dashed line), and the time-resolved vertical spot size (solid line). The time-integrated vertical spot size is 5.1 mm measured from film.

Note that the diode current and voltage in Fig. 7a are very similar to those of the quarter-wavelength focussing shown in Fig. 4a, but the dose of the ballistic focus experiment is 75% greater. This discrepancy is accounted for by difference in beam temperature, the ratio of the average non-axial velocity ($v_\perp$) of the electrons to the average total velocity (v). A high beam temperature will reduce on-axis dose, since the resulting bremsstrahlung photons will be emitted more isotropically than those from a low temperature beam. In other words, the electrons will be less forward directed, and so the x-rays will be less concentrated on axis.

A series of Monte Carlo simulations[26] were executed varying electron beam voltage, and transverse beam temperature, $\beta_\perp = v_\perp/v_{tot}$, to obtain a radiographer equation[22,27] specific to the TriMeV geometry assuming no ion component to the diode current. This radiographer equation that relates dose rate to voltage, current and $\beta_\perp$ is:

$$\dot{D} = 1020 I V^{2.6} Exp\left[-\frac{(V+0.5)\beta_\perp}{2.4}\right] \qquad (2)$$

where $\dot{D}$ is the x-ray dose rate in rad @ m/s, I is the beam current in A, V is the diode voltage in MV, and $\beta_\perp$ is the transverse beam temperature.

Figure 8 shows how $\beta_\perp$ must evolve through the pulse in order to make Equation 2 match the measured dose rate for the quarter-wavelength and ballistic focussing shots shown in Figs. 4 and 7. For both curves in Fig. 8 the electron current striking the bremsstrahlung target was

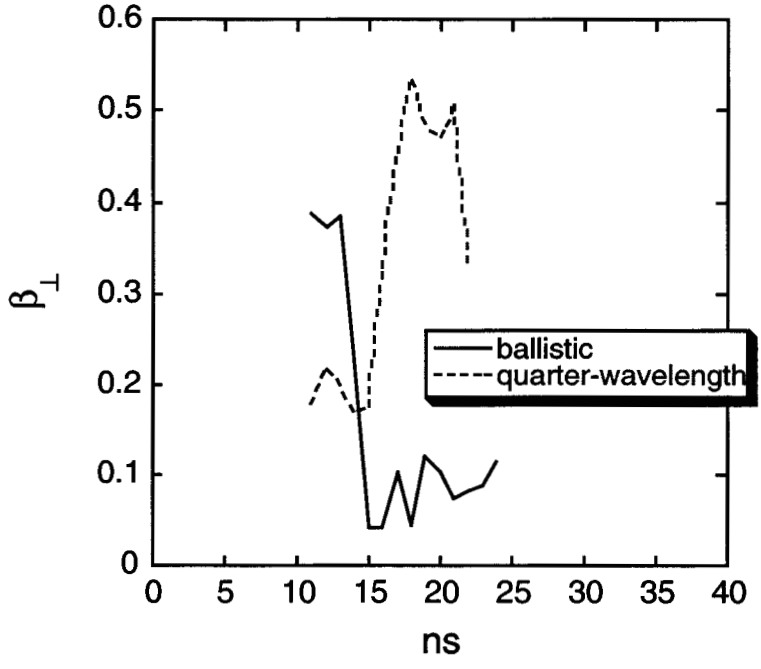

Figure 8. Calculated transverse electron beam temperature ($\beta_\perp = v_\perp/v_{tot}$) necessary to match equation 2 with measured dose rate data for the ballistic and quarter-wavelength focussing techniques. The early high temperature calculated for the ballistic focussing is due to overestimation of the electron beam current transported to the target during the initial ionization of the gas.

assumed equal to the diode current. The high $\beta_\perp$ values calculated for the ballistic focussing early in the pulse (11-13 ns) are due to overestimation of the electron current on target during the interval in which the beam front is eroded by the ionization of the gas. It is obvious from Fig. 8 that the transverse beam temperature is on average lower using the ballistic focussing method. Note also that the jump in beam temperature seen at 16-17 ns for the quarter-wavelength focussing technique also corresponds to a jump in beam size seen at the same time in Fig. 5b, perhaps indicating the onset of an instability. The fact that both methods produce nearly the same spot size makes the ballistic focussing diode radiographically superior for the parameter space probed with TriMeV.

The ballistic focussing experiments concentrated on two gases, nitrogen and neon. Figure 9 graphs the effect of gas cell drift length for 10 Torr of N_2 and 20 Torr of Ne. The IPROP code predicted an optimum drift length of 4 cm for N_2 (10 Torr), and 3.5 cm for Ne (20 Torr), which is in agreement with the results shown.

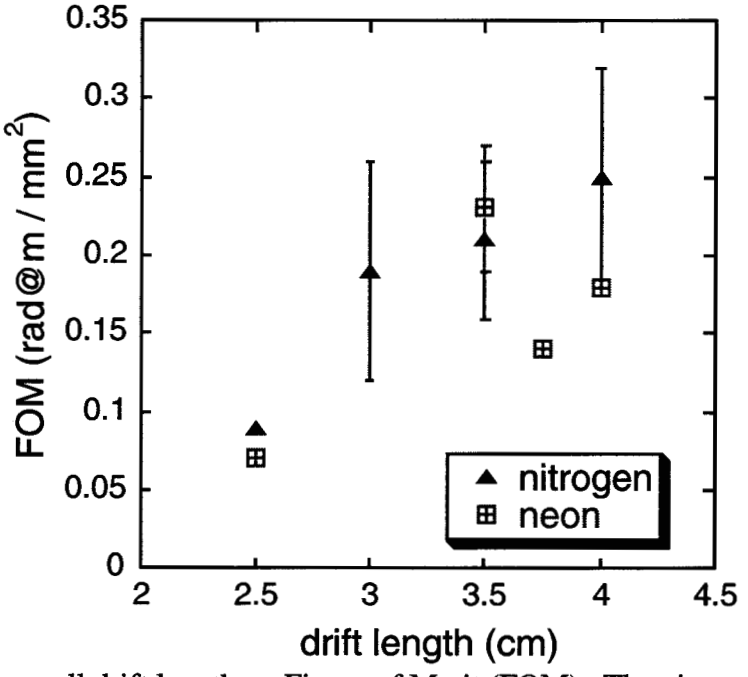

Figure 9. Effect of gas cell drift length on Figure of Merit (FOM). The nitrogen data were taken a 10 Torr, and the neon data were taken at 20 Torr. Data points without error bars indicate only one experiment performed with those parameters.

III. Magnetically Immersed Diode

A. Focussing Mechanism

The magnetically immersed diode has demonstrated the capability to produce high quality millimeter-scale radiographic sources[6,9]. The electron beam is emitted from a small diameter (< 2 mm) cathode needle and is confined to a small radius by a large solenoidal magnetic field. Previous experiments with this diode at higher energy (8-10 MV) and longer

pulse have shown unstable diode impedance and voltage degradation leading to loss of dose in accordance with Eq. 2 [22]. Moreover, the x-ray spot size was observed to grow rapidly upon the onset of the unstable impedance, causing further decrease in FOM. It was expected that TriMeV's short pulse would be completed before impedance collapse or spot growth occurred, allowing a greater FOM than the gas focussing sources.

B. Experimental Arrangement

TriMeV was operated in negative polarity for the magnetically immersed diode experiments. The high voltage electrode was modified by replacing the field-shaper terminus with a cone that tapered down to a needle as it entered the solenoid as shown in Figure 10. The profile of the cone was designed to be conformal to the contours of magnetic flux to minimize electron current injected from outside to inside of the magnet region[17]. The needle was typically 10-30 cm long, was immersed in the magnetic field and served as the electron source. The solenoid was 9 cm in diameter, 30 cm in length and could provide up to 17.5 T (pulsed, 8 mH) when driven by 13 kA (17.5 ms to peak). The AK gap could be adjusted by changing the length of either the needle or target holder. The bremsstrahlung target was a 2 cm diameter, 0.5 mm thick Ta disk, backed by a 1 cm thick graphite beam stop.

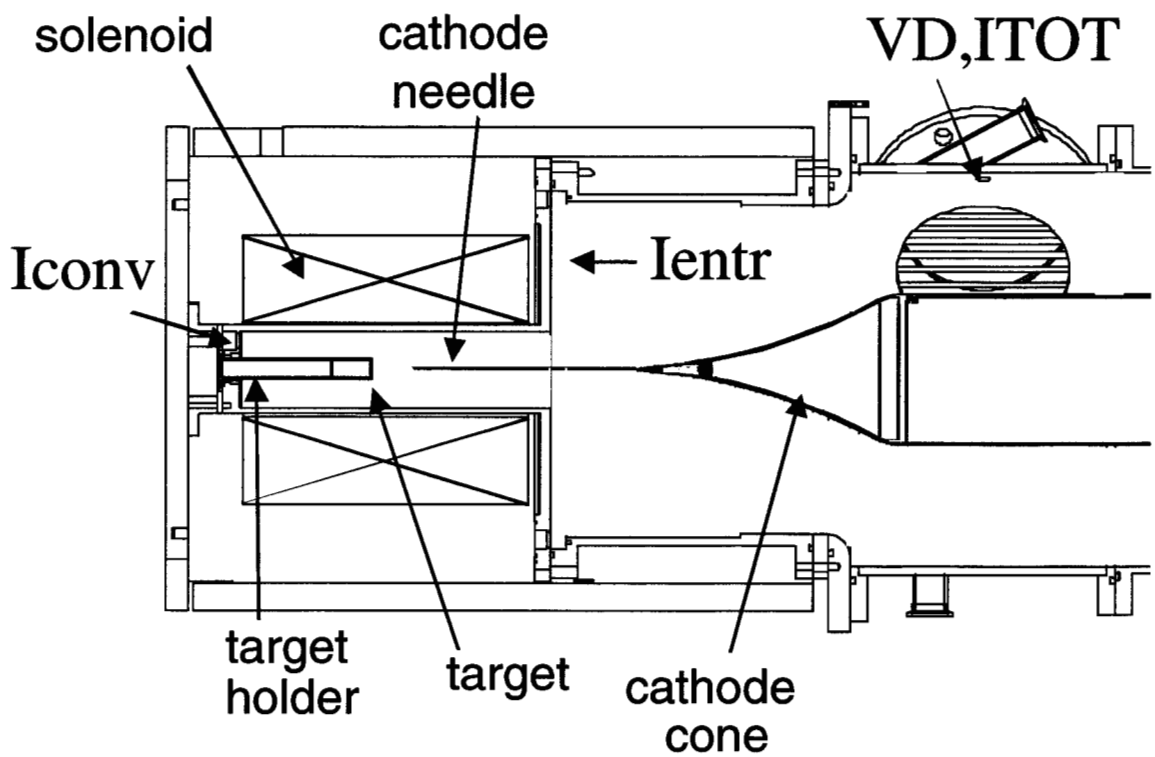

Figure 10. Schematic of the magnetically immersed diode. The center conductor of the transmission line is tapered down to a needle, immersed in a strong magnetic field, and acts as a

small diameter electron source. VD, I_{tot}, I_{conv}, and I_{entr} are accelerator diagnostics that measure voltage, total transmission line current, current entering the solenoid, and beam current at the bremsstrahlung converter, respectively.

Voltage is measured with the same probe used in the gas cell focussing experiments, labeled VD in Figs. 10 and 2. Voltage at the diode is inferred with a 160 nH inductive correction. Total current flowing in the transmission line is measured with a B-dot probe, labeled ITOT. Current entering the solenoid (Ientr), and the beam current at the bremsstrahlung converter (Iconv) are measured with two B-dot monitors each, placed 180° apart.

C. Data and Discussion

Sample data from a typical magnetically immersed shot is shown in Figure 11. Using a 5 cm AK gap (needle tip to bremsstrahlung target), 17.5 Tesla solenoidal field, 0.5 mm diameter tungsten needle, and 5 μTorr vacuum pressure. The inferred diode voltage and the x-ray dose rate are shown in Fig. 11a, producing a time integrated dose of 4.1 rad@m. The total accelerator current, ITOT, the current entering the solenoid, Ientr, and the beam current at the bremsstrahlung converter, Iconv are shown in Fig. 11b. Note Ientr and Iconv are nearly identical indicating that virtually no current is lost to the solenoid wall. The difference between the currents ITOT and Ientr represents the electron current emitted from the smaller radius portions of the cone and from the needle outside of the solenoid. This loss current is shunted to the outer wall by the return magnetic flux of the solenoid. Thus, the magnetically immersed diode operates at a higher impedance than the gas focussing diode as evidenced by the fact that the diode current (Iconv) reaches a maximum of only 15 kA, giving a minimum diode impedance of 170 Ohms at the end of the pulse flattop.

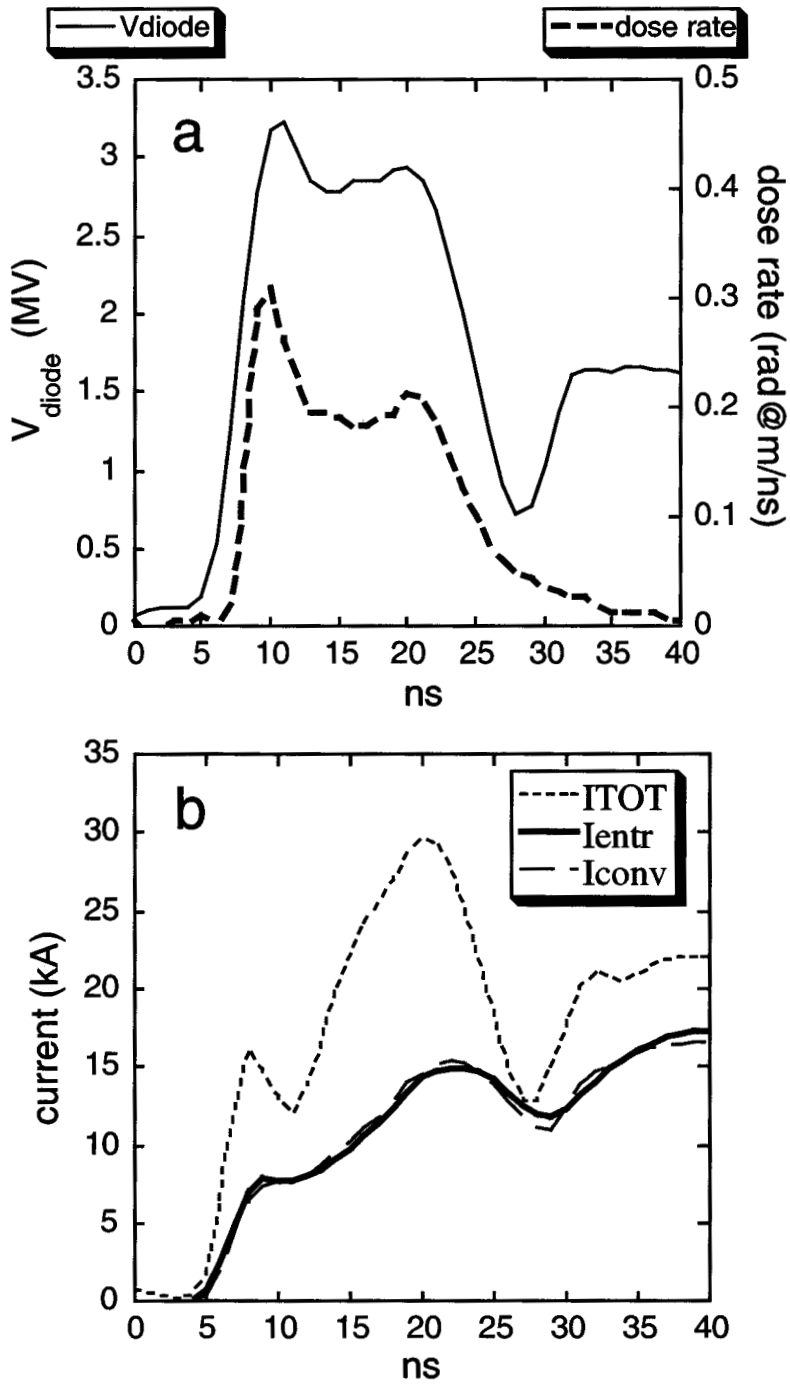

Figure 11. Data from a sample magnetically immersed diode shot. a) shows the diode voltage (solid line) and the x-ray dose rate (dashed line), which yields a time integrated dose of 4.1 rad@m. b) shows the total accelerator current (Itot, short dashes), the current entering the solenoid (Ientr, solid line), and the beam current at the bremsstrahlung converter (Iconv, long dashes).

The time-integrated spot sizes for this shot are 2.9 mm in the horizontal and 3.1 mm vertical, which is larger than expected from computer simulations[17]. Results from many

simulations predict the electron beam envelope and subsequent x-ray spot size should scale according to:

$$s = 2.6\sqrt{r_k^2 + \left(\frac{0.34T}{B}\sqrt{2\gamma\frac{I}{17kA}}\right)^2} \quad (3)$$

where s is the x-ray spot diameter in cm, r_k is the radius of the cathode needle in cm, B is the applied magnetic field in T, γ is the relativistic energy factor associated with the electrons, and I is the electron beam current in kA. This equation depicts the electron beam envelope as the needle size added in quadrature with an offset determined by the opposing strengths of the magnetic field and the spot expansion instabilities. This equation along with the time-resolved spot sizes is plotted in Figure 12. The x-ray dose rate is also shown to display relative timing. Note that initially equation 3 predicts the spot size fairly accurately, but the spot rapidly expands to over twice this value in less than 5 ns. The exact nature of this rapid spot growth is currently under investigation, but is believed to be an ion-hose type of instability[22,28]. This type of ion-hose instability is enhanced by the rapid build up of ion space charge from ions born at large radius and becoming multiply charged when reaching the electron beam path. These ions are induced from reflected primary and secondary electrons scattered out to large radius on the target face. This rapid spot growth was seen on nearly all shots taken with the magnetically immersed diode. The dose rate weighted averages of the time resolved spot size waveforms are 2.8 and 3.0 mm for the horizontal and vertical directions, respectively. The FOM for this shot is 0.49. Thus, even though x-ray spot is larger than desired, and the dose is less than in the case of ballistic gas focussing (beam current is less), the spot is small enough to double the FOM over the ballistic gas focussing method.

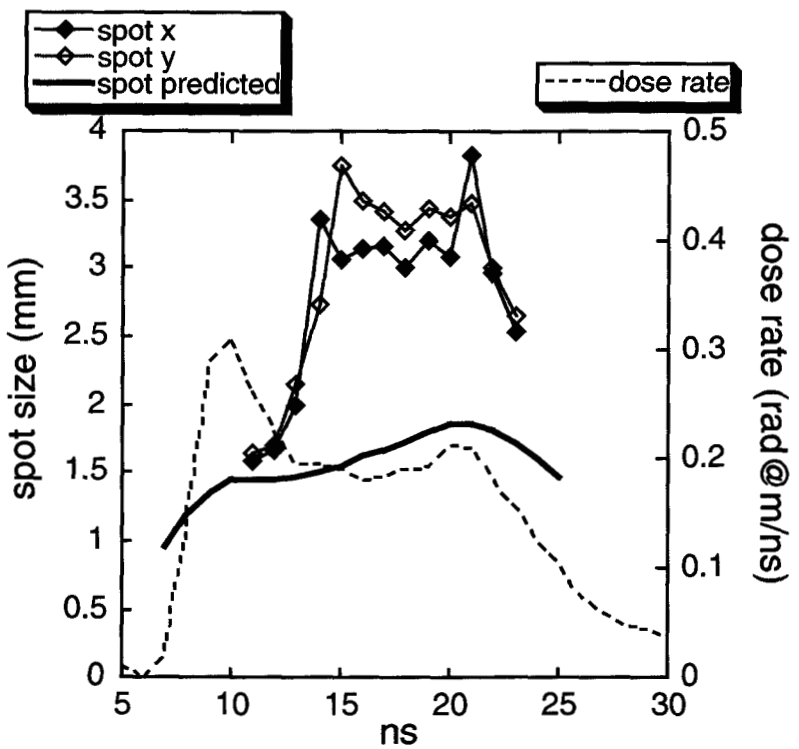

Figure 12. The experimental and predicted time-resolved spot sizes for the shot shown in the previous figure. Rapid spot growth doubling that predicted is seen . The dose rate weighted

time-integrated spots from these waveforms are 2.8, 3.0, and 1.6 mm, for the horizontal, vertical and predicted spots, respectively. The x-ray film spot was 3.0 mm average for both directions.

Many experiments were carried out to investigate the effects of changing the AK gap and the magnetic field. Figure 13a plots the FOM versus AK gap variation for solenoidal fields of 17.5 T and 0.5 mm diameter needles.

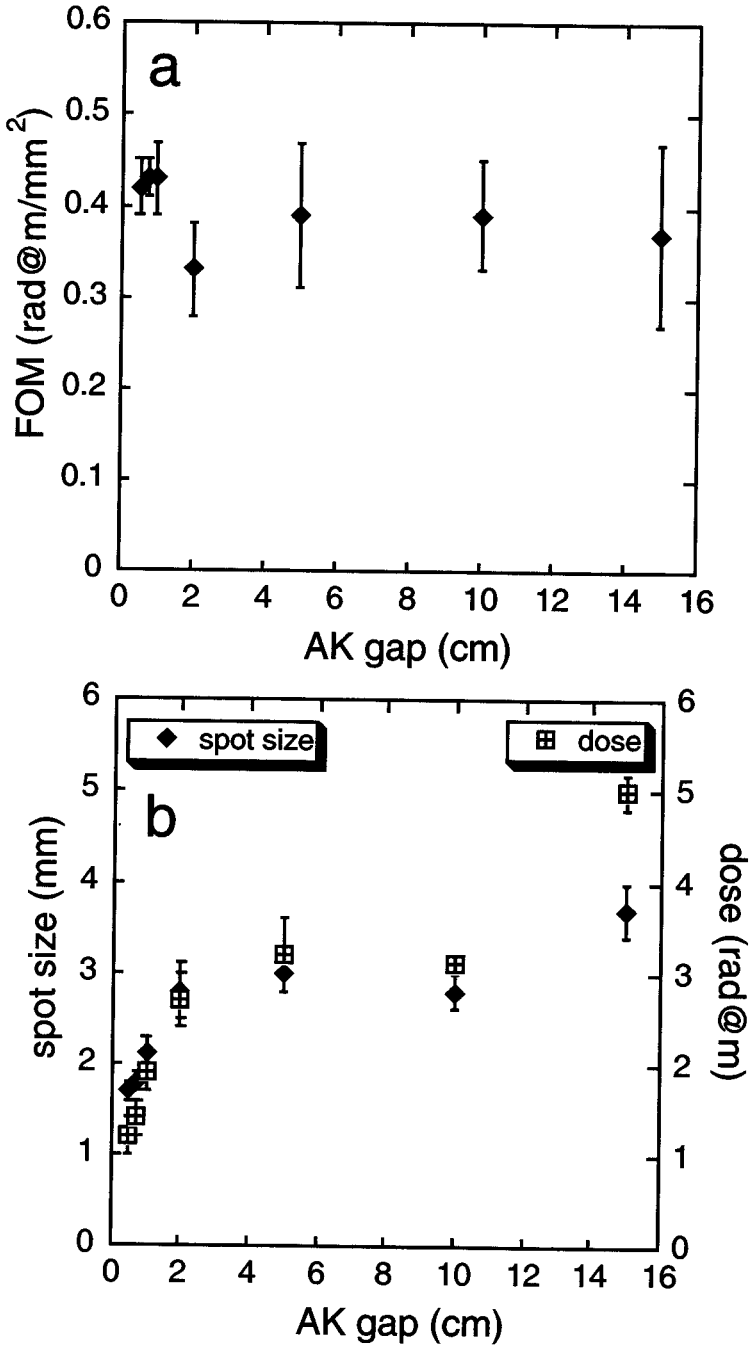

Figure 13. The effect of AK gap on FOM, spot and dose at 17.5 T. a) The FOM is relatively unaffected by changing the AK gap. b) Dose can be increased by increasing the AK gap, but spot size rises with it, causing little change in the FOM.

The first three data points are at 0.5, 0.75, and 1 cm. There is not much variability nor is there a clear trend in the data. The consistency of the FOM is especially interesting since the dose and spot size are actually varying considerably with AK gap as shown in Fig. 13b. Here, the trend is that longer AK gaps give higher dose because the diode impedance is greater and more stable, but at the cost of larger spot sizes. Short AK gaps yield small spots due to two possible reasons. The spot disrupting ion hose instability is believed to have a characteristic growth length of about 1 cm, so any gaps shorter than this should suppress the instability. Unfortunately, at gaps less than 1 cm the diode impedance collapses prior to the time that spot growth normally begins (e.g. before the 13 ns point in Fig 12). Thus, it is unresolved whether the instability is suppressed at small gaps or whether the impedance collapses before the spot can begin to grow.

Equation 3 predicts that x-ray spot size should decrease with increasing magnetic field and decreasing rod diameter. A scan of magnetic fields was performed with needle diameters of 0.5, 1, and 2 mm. The results are plotted in Fig. 14. The spot size predictions from Eq. 3 are also shown. The beam current for Eq. 3 is computed from the relativistic bipolar space charge limited current given by[29]

$$I = 17\frac{\left(\gamma^{2/3}-1\right)^{3/2}}{(1-f)\left(1+2\ln\left(r_a/r_k\right)\right)} \qquad (4)$$

Where the beam current, I, is in kA, r_a is the radius of the solenoid wall, and r_k is radius of the needle. f is the charge neutralization fraction, assumed to be 0.25 for the curves in Fig. 14. This value for the ion fraction is predicted by simulation, and its insertion into Eq. 4 correctly predicts the average current in the diode. Unfortunately, no correlation between magnetic field amplitude

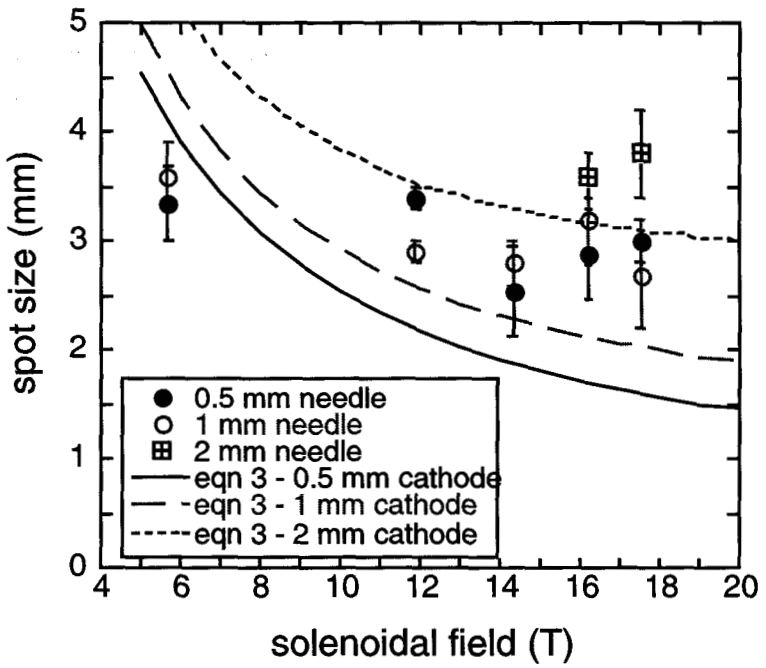

Figure 14. Effect of magnetic field and cathode needle diameter on x-ray spot size. Three needle diameters are shown: 0.5 mm (solid circles), 1 mm (open circles), and 2 mm (crossed squares). The corresponding spot size predictions from Eq. 3 are given by the curves. Note vary little spot size correlation is seen when varying the magnetic field or needle size.

and x-ray spot size appears in the experimental data. Furthermore, no improvement is seen by reducing needle size from 1 to 0.5 mm diameter. Slight improvement is seen by reducing needle size from 2 mm. The ineffectiveness of increasing B-field and decreasing needle diameter is due to the instability illustrated in Fig. 12. The beam size saturates at an approximately constant value of 3 - 3.5 mm, which does not seem dependent on magnetic field strength or needle size.

Current programmatic emphasis is on developing methods to suppress the spot enlarging instability. Three main suppression techniques are being designed for future experiments. The first is to reduce the size of the bremsstrahlung target and holder to approximately the size of the electron beam before onset of the instability. Then secondary and reflected electrons that climb to large radius must move downstream and out of the diode region to complete the circuit. Thus, no ions would be born at large radius, and any ions produced by the downstream electrons would not interfere with diode performance. The second is to heat the bremsstrahlung target to over 600° C to remove vacuum contaminants from the surface. A clean anode surface is well known to delay and reduce the ion current[30, 31]. The last method is to increase the magnetic field between the cathode and anode. Thus, the magnetic field flux lines would diverge from the perspective of an ion traveling upstream toward the needle, reducing the ion current density and removing the majority of ions from the beam path. If the instability can be properly suppressed, then a machine such as TriMeV could conceivably produce FOMs greater than 2 with the magnetically immersed diode.

IV. ROD PINCH DIODE

A. Focussing Mechanism

The rod pinch diode consists of a small diameter (< 2mm) anode rod which extends through an aperture in the cathode[15,16]. The electrons are emitted from the edges of the aperture and converge onto the anode rod. If the anode rod is of a bremsstrahlung converter material then an x-ray source suitable for radiography is created when viewed end-on. Furthermore, if properly configured, the electrons can magnetically self-insulate[32], travel down the extension and pinch at the rod tip. This mechanism can isolate the cathode and anode plasmas and thus lengthen the diode impedance lifetime relative to a geometry that terminates the anode within the cathode aperture[7,33]. The obvious advantage to this focussing scheme is that the x-ray spot will automatically be approximately the diameter of the rod. The obvious disadvantage is that the electrons will strike the rod at large angles (approximately 90°) and reduce the on-axis dose in the manner of Eq. 2 with $\beta_\perp$ approaching unity.

B. Experimental Arrangement

The natural polarity for the rod pinch is positive. This allows the anode rod to be directly attached to the center conductor of TriMeV and eliminates any reentrant features required in negative polarity. TriMeV was operated in positive polarity for the rod pinch experiments reported here. Since the vacuum insulator was designed for negative polarity, the accelerator was de-rated to ≈ 2 MV at the diode. Figure 15 illustrates the rod pinch diode configuration. A small diameter tungsten rod is fixed to the end of the transmission line center conductor. The rod approaches or penetrates through an aperture (8 or 14 mm diameter, 3 mm thick) in a cathode plate located 5 cm from the end of the center conductor. Parameters were varied to optimize FOM, including rod size and rod tip configuration (tapered or blunt). Voltage is measured with the same probe used in the gas cell focussing experiments, labeled VD. Diode current is measured with a B-dot probe, labeled ITOT.

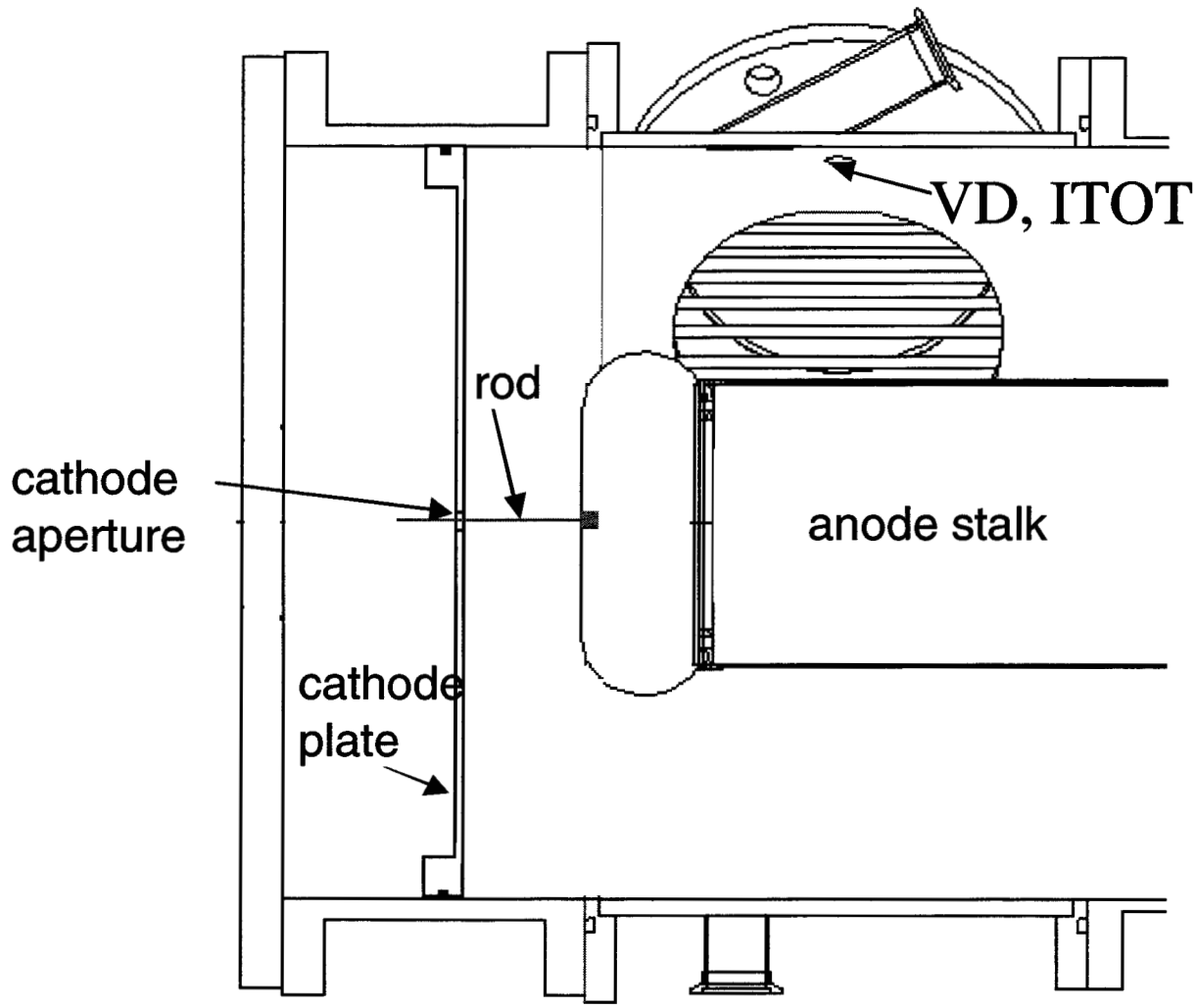

Figure 15. Schematic of the rod pinch diode. Note that the center conductor is now the anode.

C. Data and Discussion

Figure 16 shows data from a sample rod pinch diode experiment. Figure 16a graphs the voltage and diode current pulses for a diode configured with a 0.5 mm diameter tungsten rod with an untapered (blunt) tip, 8 mm diameter cathode aperture, where the rod extends 1 cm beyond the downstream edge of the cathode aperture. Note that the voltage is lower than on the previous diodes due to the necessary de-rating for positive polarity operation. However, the diode impedance is fairly high and quite steady, being 70 Ohms at the end of the pulse.

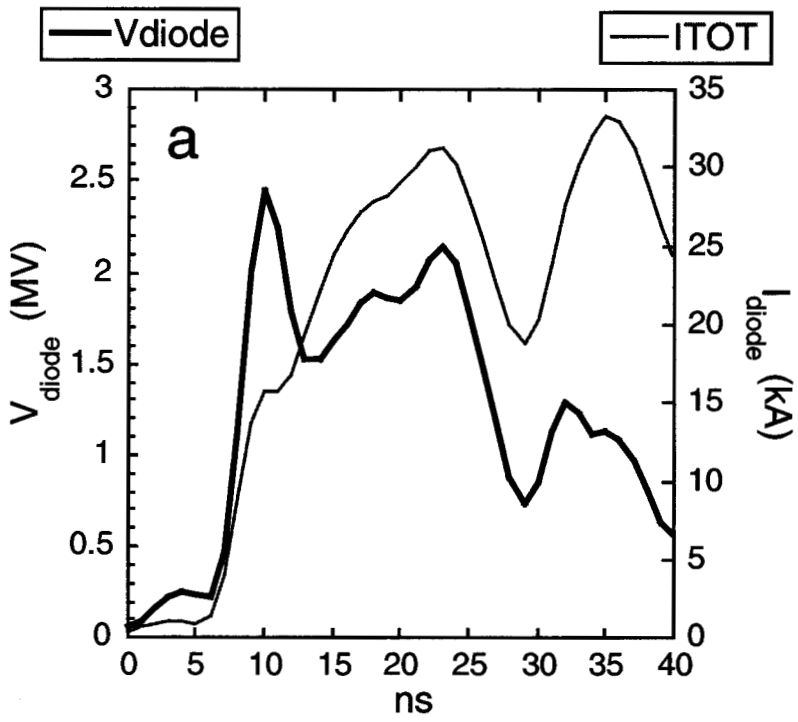

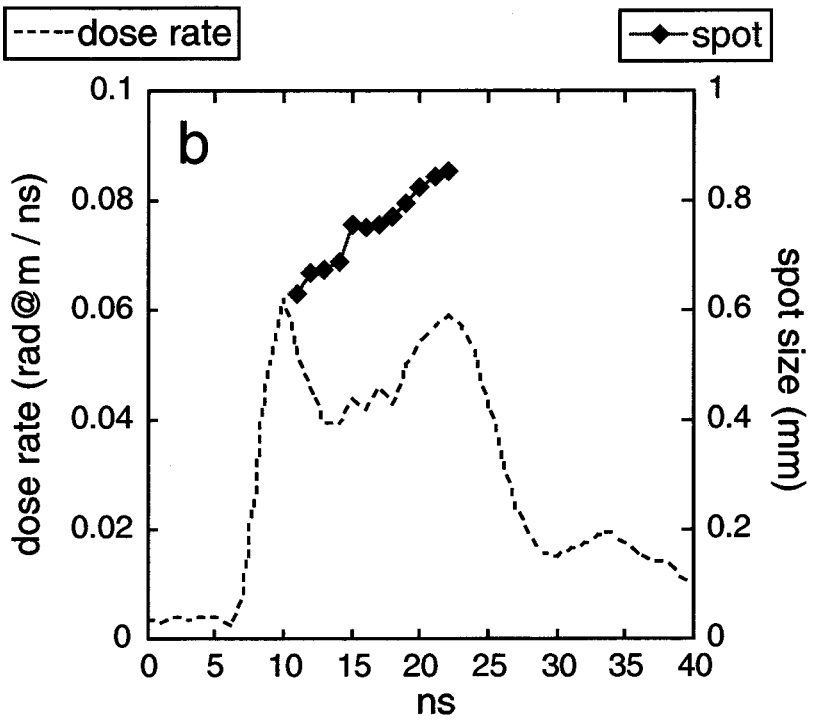

Figure 16. Data from a rod pinch diode experiment using a 0.5 mm diameter untapered tungsten rod, an 8 mm diameter cathode aperture, and a 1 cm extension beyond the aperture. a) diode voltage (thick black line) and current (thin gray line). b) dose rate (dashed line) and time-resolved spot size (gray diamonds). The continuous rise in the spot size is believed to be due to hydrodynamic expansion of the tungsten rod. This shot provided 1.2 rad@m with a 0.8 mm spot size giving FOM = 1.9.

Figure 16b shows the on-axis x-ray dose rate and the time-resolved spot size. The dose rate is much lower in comparison to the other two diode types due to lower voltage and less forward (on-axis) directivity of the bremsstrahlung, because the electrons strike the rod with near radial trajectories. The time-integrated dose from this shot is 1.2 rad@m. Note the spot size is significantly less than 1 mm. In order to measure the time-resolved spot size with adequate precision, the horizontal and vertical lines of PIN diodes described in Section II-C were combined into two adjacent vertical lines offset from each other by a half diameter. The data from the two lines were folded together to double the normal resolution to about ± 0.2 mm. The x-ray spot size is growing with time due to hydrodynamic expansion of the rod. The dose rate weighted average of the time-resolved spot size is 0.76 mm, which agrees with the time-integrated spot size of 0.80 mm measured from the film. The figure of merit for this shot is 1.9, a factor of nearly four better than the immersed diode source, and a factor of eight better than the gas focussing diode source.

Some variations on the configuration were performed to study their effects on the FOM. Specifically, the rod diameter was changed, and the effect of tapering the tip was studied. Table I lists the FOM for 0.5 and 1 mm rods, tapered and blunt (untapered). The taper used was 1 cm long to a point. When the 0.5 mm rod was tapered, the dose became very low (<0.5 rad@m). This is believed due to the rod becoming too range thin to electrons striking the taper. The CSDA range of a 2 MeV electron in tungsten is 0.9 mm. If the electrons can not connect to the rod (i.e. complete the circuit), electron space charge grows near the tip. This increases ion loss

current and can force some electrons to flow upstream away from the tip. These current constituents do not produce high energy x-rays and can decrease diode impedance and voltage causing reduction in usable dose. A dramatic collapse of diode impedance is seen with the tapered 0.5 mm diameter rods due to this mechanism, which limits the x-ray dose to less than 0.5 rad@m. Blunt 0.5 mm and 1 mm rods (tapered or blunt) do not display this impedance collapse. The blunt 0.5 mm rods produce as much dose as the 1 mm rods (typically 1 - 1.2 rad@m), but the x-ray spot sizes are significantly smaller (typically, 0.8 mm vs. 1.3 mm). Tapered 1 mm rods produce slightly smaller spots than blunt 1 mm rods (1.25 ± 0.04 mm vs. 1.33 ± 0.05 mm), hence the slightly greater FOM. Note that the 1 mm diameter rods gave more consistent results as reflected in the uncertainties.

Table I. Figures of Merit (FOM) for two different rod diameters and tip styles

		Rod diameter	
		0.5 mm	**1 mm**
Tip style	**tapered**	0.60 ± 0.30 rad@m/mm^2	0.66 ± 0.02 rad@m/mm^2
	blunt	1.65 ± 0.18 rad@m/mm^2	0.62 ± 0.04 rad@m/mm^2

V. SUMMARY AND CONCLUSIONS

Experiments were conducted on the TriMeV accelerator to determine the best type of radiography source diode in the 2 -3 MV range. Three candidate diodes were tested: Gas cell focussing with quarter-wavelength and ballistic subtypes, magnetically immersed focussing, and rod pinch focussing. The quality metric chosen for comparison was a figure of merit (FOM) defined as dose measured 1 m from the source filtered by 2.5 cm of Al, divided by the square of the x-ray source size in mm. The definition of source size diameter is described in Section I. The gas cell quarter-wavelength focussing method produced relatively large x-ray source sizes with moderate dose. The gas cell ballistic focussing method produced spot sizes similar to quarter-wavelength focussing, but with better dose due to lower beam temperature. The magnetically immersed focussing method provided moderate spot sizes and moderate dose but with a resultant FOM higher than both types of gas cell focussing. The rod pinch focussing method operated at 2/3 the voltage of the above sources produced lower doses, but with very small spot sizes and much higher FOMs. Table II lists the spots, doses, and FOMs of the best results from the candidate diodes. The rod pinch diode produced the best radiographic source by a factor of nearly 4 over that of the next best candidate, the magnetically immersed.

Table II. Best results by diode type

Diode type		Spot size (mm)	Dose (rad@m)	FOM (rad@m/mm^2)
gas cell	1/4 wavelength	5.0	3.4	0.14
	ballistic	5.1	6.0	0.23
magnetically immersed		2.9	4.1	0.49
rod pinch		0.8	1.2	1.88

An alternative method of comparison is to look at source intensity profiles. The spot profile (radial distribution of source intensity) can be unfolded from the edge spread data via reverse Abel transform[34]. Figure 17 displays the inferred x-ray spot profile for the four focussing schemes assuming azimuthal symmetry. The distributions have been weighted such that their integrals of rotation would yield the appropriate dose at 1 m from the source, thus illustrating their relative intensities. The superiority of the rod pinch focussing method is clear, making it the choice source for flash radiography at 2-3 MV.

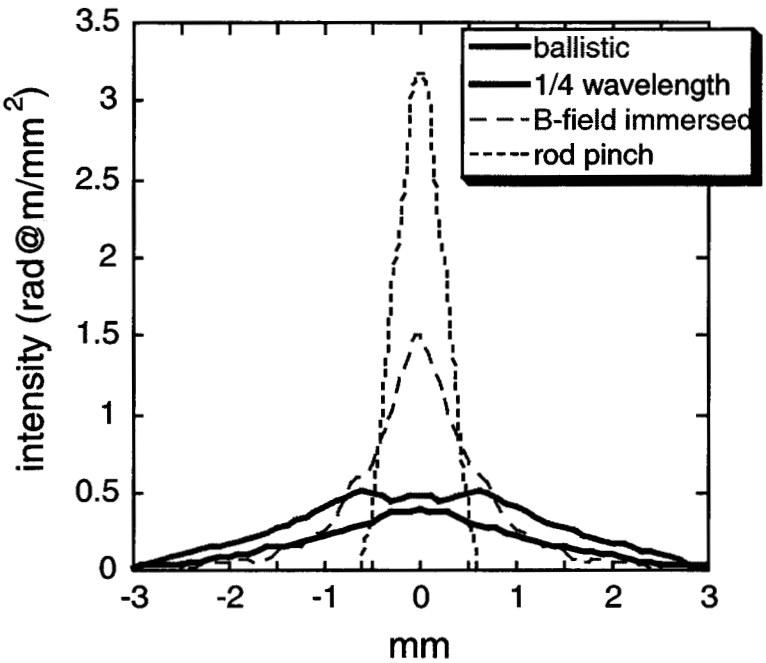

Figure 17. Time integrated spot profiles deduced from their edge spread functions for the four types of focussing for the experiments shown in Figs. 4, 7, 11, and 16. These radial distributions of source intensity have been weighted such that their integrals of rotation will yield the appropriate dose at 1 m. Note the clear superiority of the rod pinch focussing diode.

VI. REFERENCES

[1] M. Burns, P. Allison, R. Carlson, J. Downing, D. Moir, and R. Shurter, in Proceedings of the XVIII International LINAC Conference, Geneva, 1996.

_____, Los Alamos National Laboratory Report LA-UR-96-2946, 1996.

[2] M. Ong, Cavalle, R. Richardson, and J. Zentler, in *Proceedings of the 11th IEEE International Pulsed Power Conference*, edited by G. Cooperstein and I. Vitkovitsky, Baltimore, MD, June 29 - July 2, 1997, IEEE Catalog Number 97CH36127 (Institute of Electrical and Electronic Engineers, Piscataway, NJ, 1997), p. 892.

[3] AWE Pulsed Power Group, "Mogul E Flash X-ray Facility", Atomic Weapons Establishment report AWE/HD/9602/R01. Aldermaston, England (1996).

[4] M. Mouilet, R. Boivinet, F. Bombardier, J. Delvaux, E. Merle, O. Pierret, J.C. Ribes, J. Bardy, A. Devin, In IEEE Conference Record - Abstracts, 2001 IEEE International Conference on Pulsed Power Plasma Science, Las Vegas, Nevada, June 17-22, 2001, IEEE Cat. No. 01CH37255, (Institute of Electrical and Electronic Engineers, Piscataway, NJ, 2001), p. 525.

[5] F. Bayol, P. Charre, A. Garrigues, C. Gonzalez, F. Fompier, R. Vezinet, R.J. Commisso, F.C. Young, R.J. Allen, J.R. Boller, G. Cooperstein, D. Mosher, S.B. Swanekamp, In IEEE Conference Record - Abstracts, 2001 IEEE International Conference on Pulsed Power Plasma Science, Las Vegas, Nevada, June 17-22, 2001, IEEE Cat. No. 01CH37255, (Institute of Electrical and Electronic Engineers, Piscataway, NJ, 2001), p. 457.

[6] M.G. Mazarakis, J.W. Poukey, D.C. Rovang, J.E. Maenchen, S.R. Cordova, P.R. Menge, R. Pepping, L. Bennett, K. Mikkelson, D.L. Smith, J. Halbleib, W.A. Stygar, and D.R. Welch, Appl. Phys. Lett. **70** (7), p.832 (1997)

[7] D. Platts, M.P. Hockaday, D. Beck, W. Coulter, and R.C. Smith, in *Proceedings of the 10th IEEE International Pulsed Power Conference*, edited by W. Baker and G. Cooperstein, Albuquerque, NM, July 3-6, 1995, IEEE Catalog Number 95CH35833 (Institute of Electrical and Electronic Engineers, Piscataway, NJ, 1995), p. 430.

[8] Francis Jamet and Gustov Thomer, *Flash Radiography* (Elsevier Scientific, New York, 1976).

[9] John Maenchen, S. Cordova, J. Gustwiller, D.L. Johnson, P.R. Menge, I. Molina, C. Olson, S. Rosenthal, D. Rose, B. Oliver, D. Welch, V. Bailey, I. Smith, D. Droemer, E. Hunt, G. MacLeod, L. Woo, in *Proceedings of the 12th IEEE International Pulsed Power Conference*, edited by C. Stallings and H. Kirbie, Monterey, California, June 27-30, 1999, IEEE Catalog Number 99CH36358 (Institute of Electrical and Electronic Engineers, Piscataway, NJ, 1999), p. 279.

[10] A.R. Birrell, R.D. Edwards, T.J. Goldsack, and M.A. Sinclair, IEEE Trans. Plas. Sci. **28**, 1660 (2001).

[11] R.L. Carlson, M.J. George, T.P. Hughes, and D.R. Welch, in *Proceedings of the 1993 Particle Accelerator Conference*, Washington, DC, 1993, IEEE Cat. No. 93CH32797 (Institute of Electrical and Electronic Engineers, Piscataway, NJ, 1993), p.661.

[12] E. Hunt, G. MacLeod, L. Woo, D. Droemer, S. Cordova, J. Gustwiller, D. Johnson, J. Maenchen, P. Menge, I. Molina, C. Olson, S. Rosenthal, D. Rovang, B. Oliver, D. Welch, C. Eichenberger, P. Spence, I. Smith, and V. Bailey, In IEEE Conference Record - Abstracts, 1999 IEEE International Conference on Plasma Science, Monterey, California, June 20-24, 1999, IEEE Cat. No. 99CH36297, (Institute of Electrical and Electronic Engineers, Piscataway, NJ, 1999), P.181.

[13] A.E. Blaugrund and G. Cooperstein, Phys. Rev. Letts. **34**, 461 (1975)

[14] D.W. Forster, M.D. Hutchinson, "MEVEX", Atomic Weapons Research Establishment report SSWA/SWAN/790, Aldermaston, England (1979).

[15] G. Cooperstein, J.R. Boller, R.J. Commisso, D.D. Hinshelwood, D. Mosher, P.F. Ottinger, J.W. Schumer, S.J. Stephanakis, S.B. Swanekamp, B.V. Weber, and F.C. Young, "Theoretical Modeling and Experimental Characterization of a Rod-Pinch Diode," to be published in Phys. Plasmas, Oct. 2001.

[16] R.A. Mahaffey, J. Golden, Shyke A. Goldstein and G. Cooperstein, "Intense Electron-Beam Pinch Formation and Propagation in Rod Pinch Diodes," Appl. Phys. Lett., **33** (9), 795 (1978).

[17] D.R. Welch, B.V. Oliver, S.E. Rosenthal and C.L. Olson, in IEEE Conference Record - Abstracts, 1999 IEEE International Conference on Plasma Science, Monterey, California, June 20-24, 1999, IEEE Cat. No. 99CH36297, (Institute of Electrical and Electronic Engineers, Piscataway, NJ, 1999), p. 182.

[18] see for example, Stanley Humphries, Jr, *Principles of Charge Particle Acceleration* (Wiley-Interscience, New York, 1986).

[19] J.C. Martin, "Aids to Estimating the Quality of Flash Radiographs.", Atomic Weapons Research Establishment report SSWA/JCM/788/266. Aldermaston, England (1978).

[20] K.H. Mueller, L. LeDain, G. Vernier, "Methods for Determining the Diameter of the Focal Spot," Los Alamos National Laboratory report LA-UR 92-3870 (1992).

[21] D.R. Welch, C.L. Olson and T.W.L. Sanford, Phys. Plasmas **1**, 764 (1994)

[22] P.R. Menge, J.E. Maenchen, M.G. Mazarakis and S.E. Rosenthal, in *Proceedings of the 12th IEEE International Pulsed Power Conference*, edited by C. Stallings and H. Kirbie, Monterey, California, June 27-30, 1999, IEEE Catalog Number 99CH36358 (Institute of Electrical and Electronic Engineers, Piscataway, NJ, 1999), p. 1033.

[23] J.R. Pierce, *Theory and Design of Electron Beams*, (D. Van Nostrand Co., New York, 1954) Ch. 10

[24] W.A. Stygar, R.B. Spielman, H.C. Ives, W.B.S. Moore, J.F. Seamen, A.W. Sharpe, T.C. Wagoner, T.L. Gilliland, R.S. Broyles, J.A. Mills, T.A. Dinwoodie, J.S. Slopek, K.W. Struve, P.G. Reynolds, "D-dot and B-dot Monitors for Z-Vacuum-Section Power-Flow Measurements," in *Proceedings of the 11th IEEE International Pulsed Power Conference*, edited by G. Cooperstein and I. Vitkovitsky, Baltimore, Maryland, June 29-July 2, 1997, IEEE Cat. No. 97CH36127, (Institute of Electrical and Electronic Engineers, Piscataway, NJ, 1997), p. 1258.

[25] J.P. Lidestri, P.W. Spence, V.L. Bailey, S.D. Putnam, J. Fockler, C. Eichenberger, and P. D'A Champney, IEEE Trans. Plas. Sci. **19**, 855 (1991)

[26] J.A. Halbleib, R.P. Kensek, T.A. Mehlhorn, G.D. Valdez, S.M. Setzer, and M.J. Berger, IEEE Trans. Nuc. Sci., **39**, 1025 (1992).

[27] D.E. Beutler, J.A. Halbleib, T.W.L. Sanford, and D.P. Knott, IEEE Trans. Nucl. Sci. **41**, 2727 (1994).

[28] D.R. Welch, R.C. Clark, T.C. Genoni, T.P. Hughes, B.V. Oliver, "Theoretical Support for the Inductive-Voltage-Adder Radiography Program at Sandia National Laboratories," Mission Research Corporation report MRC/ABQ-R-1847 (1997)

[29] R.B. Miller, *An Introduction to the Physics of Intense Charged Particle Beams*, (Plenum Press, New York, 1982), Ch. 7.

[30] M.E. Cuneo, "The Effect of Electrode Contamination, Cleaning and Conditioning on High-Energy Pulsed-Power Device Performance," IEEE Trans. on Dielect. and Elect. Insul., **6**, 469 (1999).

[31] S.J. Stephanakis, B.V. Weber, B. Moosman, R.J. Allen, R.J. Commisso, G. Cooperstein, F.C. Young, in IEEE Conference Record - Abstracts, 2001 IEEE International Conference on Pulsed Power Plasma Science, Las Vegas, Nevada, June 17-22, 2001, IEEE Cat. No. 01CH37255, (Institute of Electrical and Electronic Engineers, Piscataway, NJ, 2001), p. 403.

[32] J.M. Creedon, "Magnetic Cutoff in High Current Diodes," J. Appl. Phys., **48**, 1070-1077 (1977).

[33] D.L. Fehl and J. Chang, Rev. Sci. Instrum. **54**, 665 (1983).

[34] see for example, J.C. Dainty and R. Shaw, *Image Science*, (Academic Press, New York, 1974), Ch. 6.

DISTRIBUTION:

5	MS	1193	J.E. Maenchen, 1645
1		1193	D.C. Rovang, 1645
1		1193	D.L. Johnson, 1645
1		1193	I. Molina, 1645
1		1193	J. Woodworth, 1645
1		1194	D.H. McDaniel, 1640
2		0899	Technical Library, 9616
1		0612	Review and Approval Desk, for DOE/OSTI, 9612
1		9018	CTF, 8945-1

3 Mission Research Corporation
Attn: D.R. Welch
B.V. Oliver
D.V. Rose
5001 Indian School Rd NW
Albuquerque, NM 87110

2 Naval Research Laboratory
Attn: G. Cooperstein
R. Commisso
4555 Overlook Ave. SE
Washington, DC 20375

4 Los Alamos National Laboratory
Attn: R.D. Fulton
N.S. King
M.D. Wilke
D.M. Oro
P.O. Box 1663
Los Alamos, NM 87545

3 Atomic Weapons Establishment
Attn: T. Goldsack
Aldermasteon, Reading RG7 4PR
Berkshire
ENGLAND

3 Bechtel-Nevada
Attn: E. Hunt
G. MacLeod
D. Droemer
P.O. Box 98521
Las Vegas, NV 89193-8521

2 Titan Pulse Science
Attn: I. Smith
V. Bailey
600 McCormick St.
San Leandro, CA 94577